2010 IEEE International Conference on Robotics and Automation
Anchorage Convention District
May 3-8, 2010, Anchorage, Alaska, USA

A Hovering Control Strategy for a Tail-Sitter VTOL UAV that Increases Stability Against Large Disturbance

Takaaki Matsumoto*1, Koichi Kita*2, Ren Suzuki*1, Atsushi Oosedo*1,
Kenta Go*1, Yuta Hoshino*1, Atsushi Konno*1 and Masaru Uchiyama*1
*1Department of Aerospace Engineering, Tohoku University.
Aoba-yama 6-6-01, Sendai, Miyagi, 980-8579, Japan
*2Fuji Heavy Industries Ltd., 1-1-11
Yonan, Utsunomiya, Tochigi, 320-8564, Japan
{takaaki, konno, uchiyama}@space.mech.tohoku.ac.jp, KitaK@uae.subaru-fhi.co.jp

***Abstract*— The application range of UAVs (unmanned aerial vehicles) is expanding along with performance upgrades. Vertical take-off and landing (VTOL) aircraft has the merits of both fixed-wing and rotary-wing aircraft. Tail-sitting is the simplest way for the VTOL maneuver since it does not need extra actuators. However, conventional hovering control for a tail-sitter UAV is not robust enough against large disturbance such as a blast of wind, a bird strike, and so on. It is experimentally observed that the conventional quaternion feedback hovering control often fails to keep stability when the control compensates large attitude errors. This paper proposes a novel hovering control strategy for a tail-sitter VTOL UAV that increases stability against large disturbance. In order to verify the proposed hovering control strategy, simulations and experiments on hovering of the UAV are performed giving large attitude errors. The results show that the proposed control strategy successfully compensates initial large attitude errors keeping stability, while the conventional quaternion feedback controller fails.**

I. INTRODUCTION

VTOL UAVs make missions possible which are normally impossible to accomplish using either fixed-wing or rotary-wing UAVs alone; for example, search and rescue operations covering a broad area located at the rooftop of a building. There are several ways to perform VTOL maneuvers such as tilting-rotor, tilting-wing, thrust-vectoring and tail-sitting etc. The simplest way is tail-sitting since it does not need extra actuators for the VTOL maneuver. A simple mechanism is preferable for UAVs, because weight saving is crucial for the VTOL maneuver and has the advantage of cost saving. Tail-sitter VTOL aircraft switches between level flight mode and hover mode by changing the pitch attitude of the fuselage by 90 ° as shown in Fig. 1.

US Air Force Research Lab and AeroVironment Inc. have developed "SkyTote" which is equipped with a coaxial contra-rotating propeller [1]. The Defense Advanced Research Projects Agency (DARPA) and Aurora Flight Sciences have developed "GoldenEye" which is equipped with a ducted fan. It uses fins outside the duct during level flight and fins in the duct during hovering [2]. Stone developed "T-Wing" which has a canard wing and tandem rotors [3],[4]. Kubo and Suzuki proposed a twin-fuselage plane [5]. Green and Oh developed a micro air vehicle [6], and added two wingtip rotors which generate a rotational force countering the motor torque to their MAV [7].

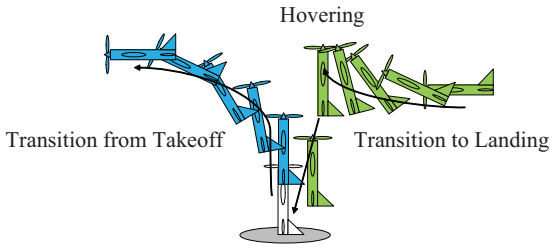

Fig. 1. Takeoff and landing of the tail-sitter VTOL aircraft.

However, those tail-sitter UAVs have some complex equipments such as a coaxial contra-rotating propeller [1], a ducted fan and fins [2], side-by-side rotors [4],[5], and wingtip rotors [7] for the tail-sitting VTOL maneuver.

Only few attempts have been made to develop tail-sitter UAVs without any extra equipment so far. However, since these simple tail-sitter UAVs have no extra equipment for countering the motor torque, robust stationary hovering is more difficult than other robots with complex equipments. Large disturbances in hovering such as strong wind or bird impact are major problems to overcome.

Frank et al. have succeeded in the indoor flight experiment using a commercially available R/C acrobatic airplane and the motion capture system [8]. However, since the flight experiments were performed in a room, there was no disturbance such as strong wind which is a major problem to overcome [8]. Knoebel et al. proposed a new airframe design [9]. They are working on flight tests using a commercially available single propeller R/C model which represents the "XFY1". However, hovering performance with large disturbance were not reported in [9]. Johnson et al. have developed "GTEdge" which is a large scale R/C airplane weighting about 15 kg and studied the tail-sitter maneuver [10],[11]. They have succeeded transition flight and hovering; however, the robustness of hovering control was not discussed.

This paper is intended to propose a novel control strategy for robust hovering when large attitude errors are generated by some disturbances. Simulations and experiments on hovering control of the UAV are performed giving large attitude

Fig. 2. Tail-Sitter UAV.

errors to verify the robustness against the errors. The results show that the proposed strategy successfully compensates the large errors, while the conventional control strategy failed to stabilize the UAV. The UAV used in this paper is equipped with all necessary sensors and computers on the fuselage [12].

II. SYSTEM CONFIGURATION

An overview of the tail-sitter VTOL UAV is shown in Fig. 2. The main wingspan is 1.0 m, and the weight is 0.75 kg. The main and tail wings are parts of commercially available R/C airplane (Hyperion Co., Sniper 3D), and other parts such as the body are newly developed. The motor and propeller, of which the static thrust amounts to 120 % of the fuselage weight at a continuous maximum motor load are selected.

The UAV is equipped with the following processors and sensors.

- A microcomputer board (Alpha Project Co., STK-7125) that has an SH2 microcomputer made by Renesass Technology Co. The microcomputer calculates control input based on each sensor data, and sends pulse-width modulated (PWM) signals to servo motors to control surfaces (aileron, elevator, and rudder) and the thrust motor.
- An attitude sensor module (Microstrain Co., 3DM-GX1). This module provides the attitude, azimuth, three-axis angular velocity and acceleration. The sensor's datasheet gives its attitude angle accuracy as ± 2 °.
- An ultrasonic sensor to detect altitude when the aircraft's distance from the ground is less than 6 m.
- An atmospheric pressure sensor to detect altitude when aircraft distance from the ground is more than 6 m.
- A global positioning system (GPS) receiver module (Garmin Co., GPS 18-5Hz). The GPS module obtains absolute position on the earth and absolute velocity of the three axes.
- A micro-SD card module to record flight data and other information for postexperiment analysis.
- A R/C receiver to control aircraft by a human in emergency. The main computer receives commands from an R/C transmitter, but these are not used in control calculation.

A configuration diagram of the electronic system is shown in Fig. 3.

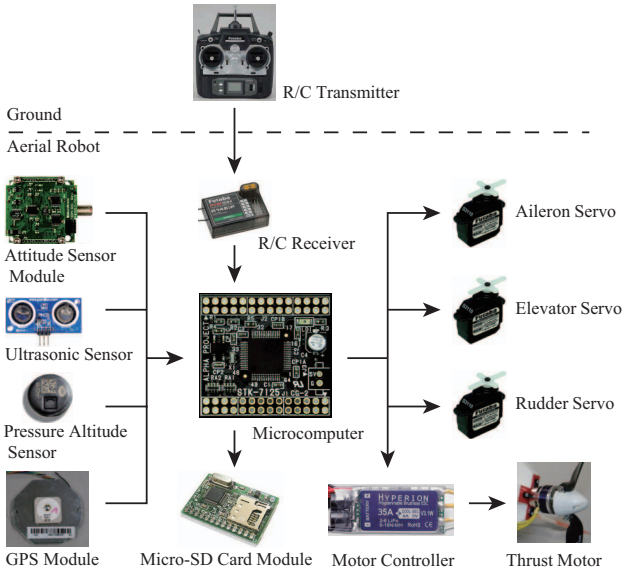

Fig. 3. On-board electronics system.

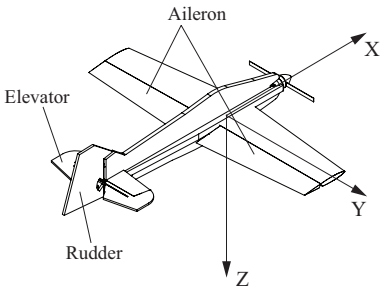

Fig. 4. Aircraft body coordinates and control surfaces.

III. HOVERING CONTROL

A. Quaternion Feedback Control

The earth fixed coordinate system defines X axis as true north, Y axis as east, and Z axis as perpendicular downward. The fuselage fixed coordinate system is defined as shown in Fig. 4 as a principal axis of inertia. The attitude of the fuselage is expressed with respect to the earth fixed coordinate system.

Because the tail-sitter maneuver covers a wide range of attitudes, quaternion expression which theoretically has no singularity is used as a method of describing the attitude. Quaternion expresses the attitude by a three dimensional unit vector $\boldsymbol{r}$ and its rotation angle ζ, as follows:

$$\boldsymbol{q} = \begin{bmatrix} \cos(\zeta/2) \\ \boldsymbol{r}\sin(\zeta/2) \end{bmatrix} = [q_0\ q_1\ q_2\ q_3]^T . \tag{1}$$

Quaternion feedback is generally used for UAVs. In controlling the attitude of the UAV, following three quaternions are defined: $\boldsymbol{q}_r$ that shows the desired reference attitude, $\boldsymbol{q}_c$ that shows the current attitude, and $\boldsymbol{q}_e$ that shows the error or deviation between $\boldsymbol{q}_r$ and $\boldsymbol{q}_c$. The $\boldsymbol{q}_e$ is shown as follows

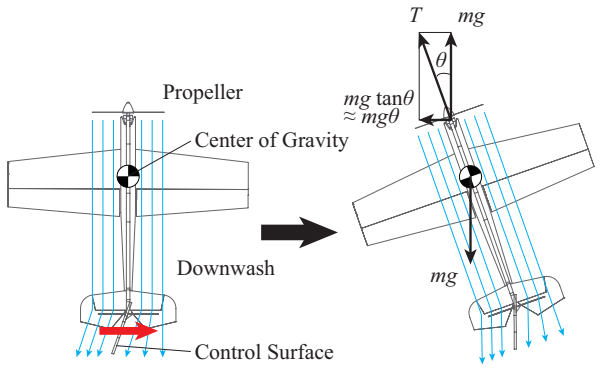

Fig. 5. Operating principle for hovering.

by using $\boldsymbol{q}_c$ and $\boldsymbol{q}_r$ [13]:

$$\boldsymbol{q}_e = \begin{bmatrix} q_{r0} & q_{r1} & q_{r2} & q_{r3} \\ -q_{r1} & q_{r0} & q_{r3} & -q_{r2} \\ -q_{r2} & -q_{r3} & q_{r0} & q_{r1} \\ -q_{r3} & q_{r2} & -q_{r1} & q_{r0} \end{bmatrix} \boldsymbol{q}_c, \tag{2}$$

where $\boldsymbol{q}_r = [q_{r0} \;\; q_{r1} \;\; q_{r2} \;\; q_{r3}]^T$. The vector part of $\boldsymbol{q}_e$ (q_{e1}, q_{e2}, q_{e3}) calculated by (2) shows amount of error about each axis in the body coordinates.

Each three axes are controlled by a PID controller. The control command is sent to control surfaces corresponding to each axis as follows:

$$\delta_i = -2(K_P q_{ei} + K_I \int q_{ei} dt + K_D \dot{q}_{ei}), \tag{3}$$

where δ_1, δ_2 and δ_3 are the aileron angle, elevator angle and rudder angle, respectively. The PID gains are provided by the ultimate sensitivity method, and tuned by trial and error. The attitude is operated by blowing a slip stream of the propeller to each control surface as shown in Fig. 5.

B. Resolved Tilt-Twist Angle Feedback Control

Quaternion feedback works well when attitude errors are not very large. However, when the rolling error is large, the quaternion feedback control presented in the previous section may fail to stabilize the UAV.

For example, let $(\alpha \;\beta \;\gamma) = (0\; 90\; 0)$ ° in a reference attitude and let $(\alpha \;\beta \;\gamma) = (180\; 80\; 0)$ ° be the current attitude, where α, β, and γ are ZYX Euler angles (yaw, pitch, and roll, respectively). In this case, the error quaternion is calculated as $[0 \;\; -0.57 \;\; 0 \;\; -0.34]^T$. This error quaternion derives no error around the Y axis of the aircraft body coordinates. Therefore, the pitch error (error around Y axis) is not compensated in the beginning of the quaternion feedback control.

We propose a novel hovering control strategy based on an analogy of inverted pendulum to achieve robustness against large attitude errors. The proposed hovering control strategy is named *Resolved tilt-twist angle control*. In this control, attitude error is resolved into the tilt and twist angles. The tilt angle is composed of two angles of orthogonal axes. Fig. 6 shows the concept of the control. The resolved tilt-twist angle control is composed of the following four steps.

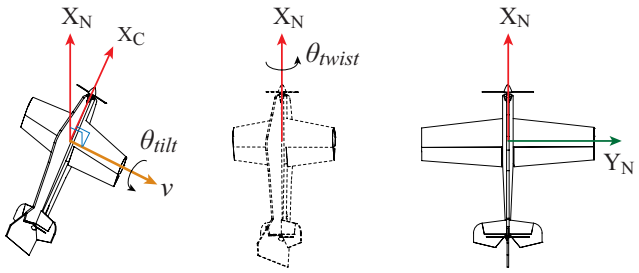

(a) Step 1. Tilt (Current Attitude) (b) Step 2. Twist (c) Reference Attitude

Fig. 6. Concept of the resolved tilt-twist angle control.

Step 1 **Derive pitch and yaw errors based on an analogy of inverted pendulum**

The first step derives the pitch and yaw errors. Current attitude ${}^O_C\boldsymbol{R}$ and reference attitude ${}^O_N\boldsymbol{R}$ of the UAV are defined as follows:

$${}^O_C\boldsymbol{R} \equiv [\boldsymbol{e}_{x_C} \; \boldsymbol{e}_{y_C} \; \boldsymbol{e}_{z_C}], \tag{4}$$

$${}^O_N\boldsymbol{R} \equiv [\boldsymbol{e}_{x_N} \; \boldsymbol{e}_{y_N} \; \boldsymbol{e}_{z_N}], \tag{5}$$

where $\boldsymbol{e}_{jC}$ and $\boldsymbol{e}_{jN}$ $(j = x, y, z)$ are the unit vectors along j axis of the body coordinate frame with respect to the world coordinate frame at current attitude and reference attitude, respectively.

Considering the UAV as an inverted pendulum, its error angles can be calculated. The attitude of inverted pendulum is defined as follows,

$$\boldsymbol{R}_E = {}^O_N\boldsymbol{R}^T \, {}^O_C\boldsymbol{R} = \begin{bmatrix} r_{11_E} & r_{12_E} & r_{13_E} \\ r_{21_E} & r_{22_E} & r_{23_E} \\ r_{31_E} & r_{32_E} & r_{33_E} \end{bmatrix}. \tag{6}$$

The X axis elements of $\boldsymbol{R}_E$ gives pitch and yaw errors as follows,

$$\theta_Y = \operatorname{atan2}(r_{31_E}, r_{11_E}), \tag{7}$$

$$\theta_Z = \operatorname{atan2}(r_{21_E}, r_{11_E}), \tag{8}$$

where $\operatorname{atan2}(y, x)$ is a function that calculates $\tan^{-1}(y/x)$. θ_Y and θ_Z define the tilt angle of inverted pendulum θ_{tilt} as follows:

$$\theta_{tilt} = \sqrt{\theta_Y^2 + \theta_Z^2}. \tag{9}$$

Step 2 **Derive roll error**

The second step derives the roll error. The rotation of θ_{tilt} is given by Rodrigues' rotation formula as follows,

$$\boldsymbol{R}_v = \begin{cases} \boldsymbol{E} + \hat{\boldsymbol{v}} \sin\theta_{tilt} + \hat{\boldsymbol{v}}^2 (1 - \cos\theta_{tilt}), & \text{for } \boldsymbol{R}_E \neq \boldsymbol{E} \quad \text{(10a)} \\ \boldsymbol{E}, & \text{for } \boldsymbol{R}_E = \boldsymbol{E} \quad \text{(10b)} \end{cases}$$

where $\boldsymbol{E}$ is a 3×3 identity matrix, $\boldsymbol{v}$ is the rotation axis vector given by the normalized cross product of $\boldsymbol{e}_{x_C}$ and $\boldsymbol{e}_{x_N}$ as follows,

$$\boldsymbol{v} = \frac{\boldsymbol{e}_{x_C} \times \boldsymbol{e}_{x_N}}{|\boldsymbol{e}_{x_C} \times \boldsymbol{e}_{x_N}|} \equiv [v_x \; v_y \; v_z]^T. \tag{11}$$

The hat operator transforms a vector $\boldsymbol{v}$ into a skew-symmetric matrix as follows,

$$\hat{\boldsymbol{v}} = \begin{bmatrix} 0 & -v_z & v_y \\ v_z & 0 & -v_x \\ -v_y & v_x & 0 \end{bmatrix}. \tag{12}$$

The UAV attitude after compensating θ_{tilt} (see the Fig. 6(b)), is given using $\boldsymbol{R}_v$ as follows:

$$\boldsymbol{R}_P = \boldsymbol{R}_v \, {}^{O}_{C}\boldsymbol{R} \equiv [\boldsymbol{e}_{x_P} \, \boldsymbol{e}_{y_P} \, \boldsymbol{e}_{z_P}], \tag{13}$$

where e_{jP} $(j = x, y, z)$ are the unit vectors along j axis of the body coordinate frame after compensating θ_{tilt} with respect to the world coordinate frame. The absolute roll error is defined as follows,

$$\theta_{twist} = \cos^{-1}\left(\frac{\boldsymbol{e}_{z_P} \cdot \boldsymbol{e}_{z_N}}{|\boldsymbol{e}_{z_P}||\boldsymbol{e}_{z_N}|}\right). \tag{14}$$

Since aircraft roll angle range is $-180\,^\circ \sim 180\,^\circ$, the sign of the roll error must be identified. In order to identify the sign of the roll error θ_X, θ_{sign} is defined as follows:

$$\theta_{sign} = \cos^{-1}\left(\frac{\boldsymbol{e}_{y_P} \cdot \boldsymbol{e}_{z_N}}{|\boldsymbol{e}_{y_P}||\boldsymbol{e}_{z_N}|}\right). \tag{15}$$

Using θ_{sign}, the roll error θ_X of the UAV is identified as follows:

$$\theta_X = \begin{cases} \theta_{twist}, & \text{for } \theta_{sign} \le \frac{\pi}{2} \quad (16a) \\ -\theta_{twist}. & \text{for } \theta_{sign} > \frac{\pi}{2} \quad (16b) \end{cases}$$

Step 3 **Projection of pitch and yaw errors onto the rolling body coordinate frame**

In order to simultaneously compensate pitch, yaw, and roll errors, the pitch and yaw errors must be projected onto the body coordinate frame which is rolling with respect to the world coordinate frame. Errors around each axis in the aircraft body coordinates are given as follows:

$$\begin{bmatrix} d_1 \\ d_2 \\ d_3 \end{bmatrix} = \begin{bmatrix} 1 & 0 & 0 \\ 0 & \cos\theta_X & -\sin\theta_X \\ 0 & \sin\theta_X & \cos\theta_X \end{bmatrix} \begin{bmatrix} \theta_X \\ \theta_Y \\ \theta_Z \end{bmatrix}. \tag{17}$$

Step 4 **Feedback control for each control surface**

Control command is sent to control surfaces based on individual axes as follows:

$$\delta_i = -(K_P d_i + K_I \int d_i dt + K_D \dot{d_i}), \tag{18}$$

where δ_1, δ_2 and δ_3 are the aileron angle, elevator angle and rudder angle, respectively. $d_1 \sim d_3$ are calculated by (17). PID gains are same as the quaternion PID feedback gains.

C. Altitude Control

The altitude controller is independently designed. The desired propeller reference rotation speed is calculated from the reference and current altitudes. Altitude control is generally possible without propeller rotation speed feedback, but control performance is deteriorated by changes in battery conditions and motor load due to disturbance. Therefore, a feedback control of propeller rotation speed is introduced in altitude control system to enhance robustness against these changes. Control gains of the altitude control system were determined through simulation.

IV. SIMULATION

A. Mathematical Model

To evaluate the hovering algorithms, a two-dimensional tail-sitter UAV simulator was developed. The translational mathematical model of the UAV in the aircraft body coordinates is represented as follows,

$$m\left(\dot{U} + QW\right) = L\sin\alpha - D\cos\alpha - mg\sin\theta + T - D_P, \tag{19}$$

$$m\left(\dot{W} - QU\right) = -L\cos\alpha - D\sin\alpha + mg\cos\theta, \tag{20}$$

where U and W are velocities along the X and Z axes in the aircraft body coordinates, L and D are lift and drag forces, α is the attack angle, θ is the pitch angle, m is the fuselage mass, g is the gravitational acceleration, T is the thrust force, D_P is the propeller drag force, and Q is the angular velocity of the Y axis around the aircraft body coordinates.

The rotational mathematical model of the UAV is represented as follows,

$$I_{xx}\dot{P} + C_p P = M_a + M_p, \tag{21}$$

$$I_{yy}\dot{Q} + C_q Q = M_t + M_e, \tag{22}$$

where P and Q are angular velocities around the X and Y axes of the aircraft body coordinates, I_{xx} and I_{yy} are inertia around the X and Y axes of the aircraft body coordinates, C_p and C_q are viscous resistance coefficients, M_a and M_p are the aileron and propeller rolling momentum around the X axis of the aircraft body coordinates, M_t and M_e are fuselage and elevator pitching momentums around the Y axis of the aircraft body coordinates.

To identify aerodynamic forces $(L, D, D_p, M_a, M_p, M_t, M_e)$, experiments including wind tunnel test are performed with scale model of the UAV. Coefficients of main wing aerodynamic forces (C_L, C_D, C_{M_t}) are measured in all attack angle range $(-180\,^\circ \sim 180\,^\circ)$. Inherent parameters of the propeller are measured through wind tunnel test. The momentum theory is used for its aerodynamic force calculation. Electrical and mechanical time constants of the DC motor are identified by experiment.

B. Simulation Results

A typical hovering simulation result of quaternion feedback is shown in Fig. 7. The initial attitude is (α β γ) = (0 0 90) $^\circ$ and the reference attitude is (α β γ) = (170 0 80) $^\circ$, where α, β, and γ are ZXY Euler angles. The error angle around Z axis decreased rapidly. However, note that the error angle around Y axis increased in the early stage

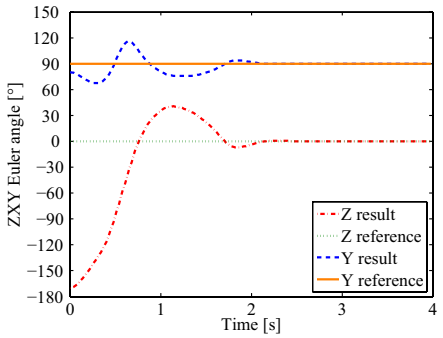

Fig. 7. Quaternion feedback control simulation.

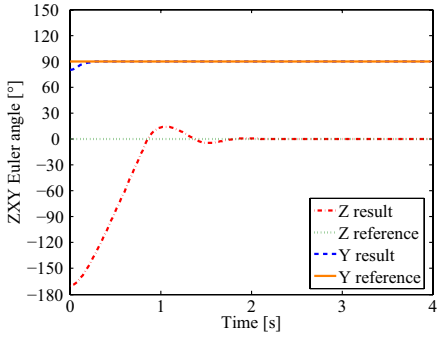

Fig. 8. Resolved tilt-twist angle control simulation.

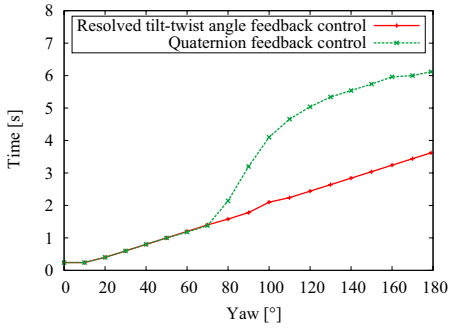

Fig. 9. Simulated recovery time comparison resolved tilt-twist angle control with quaternion feedback control.

of simulation. This error increase causes a long horizontal movement.

Fig. 8 is the result of simulation on a resolved tilt-twist angle control hovering. Same conditions are given in both simulations. The deceleration in error angle around Z axis is slightly slower than quaternion feedback. Nevertheless, the error angle around Y axis deceleration is very fast. As a result, with short horizontal movement, stable hovering is realized.

Fig. 9 shows a comparison of recovery times of both the strategies. In quaternion feedback control, when the error angle around Z axis surpasses approx 70 °, the recovering time increased exponentially. On the other hand, in resolved tilt-twist angle control, the rate of increase of recovering time is linear. Therefore, resolved tilt-twist angle control has superior stability against the large error angle around Z axis. Furthermore, the error angle around Y axis was converged very quickly in resolved tilt-twist angle feedback in all error angle ranges around Z axis. However, in quaternion feedback, the larger the error angle around Z axis exists, the longer the error angle around Y axis converge time is needed.

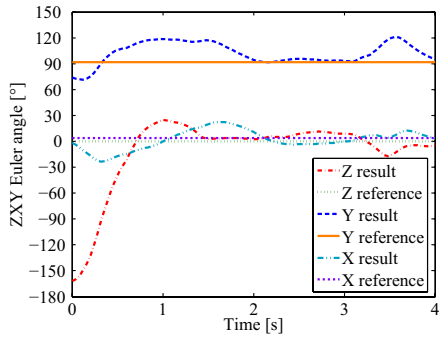

Fig. 12. Quaternion feedback control experiment.

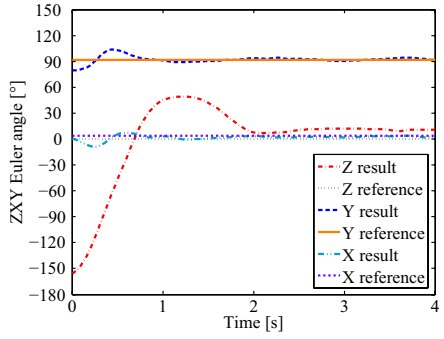

Fig. 13. Resolved tilt-twist angle control experiment.

V. EXPERIMENTAL RESULTS

A. Hovering with Quaternion Feedback Control

Fig. 10 shows snapshots of one of the hovering experiments with quaternion feedback control. In this experiment, the reference and initial attitudes are about the same as simulation. The result of the experiment is shown in Fig. 12. In the beginning of experiment, the error angle around Y axis increased and the UAV lost stability. This result is the same as the computer simulation. Moreover, the error angle around Y axis increase and the error angle around Z axis decrease caused the error angle around X axis. As a result, the UAV couldn't continue hovering.

It is notable that quaternion feedback control works well when errors are not very large. However, in some cases as shown in Fig. 10, quaternion feedback control causes problem.

B. Hovering with Resolved Tilt-Twist Angle Feedback Control

Fig. 11 shows snapshots of one of the hovering experiments with resolved tilt-twist angle control. The experiment conditions are largely similar to the quaternion feedback expriment. The result of the experiment is shown in Fig. 13. The angles around Y and X kept reference values, respectively. The error angle around Z axis decreases smoothly. This arises from independent calculation steps for tilt and twist angles in resolved tilt-twist angle control.

Additionally, even when a human inflicted large disturbance during hovering the UAV continued stable flight and errors were converged (Figs. 14 and 15). This robustness will be effective in order to overcome dynamic disturbance like a bird strike during hovering. These flights are experimented indoors, but the strategies brought out same performance in the open air.

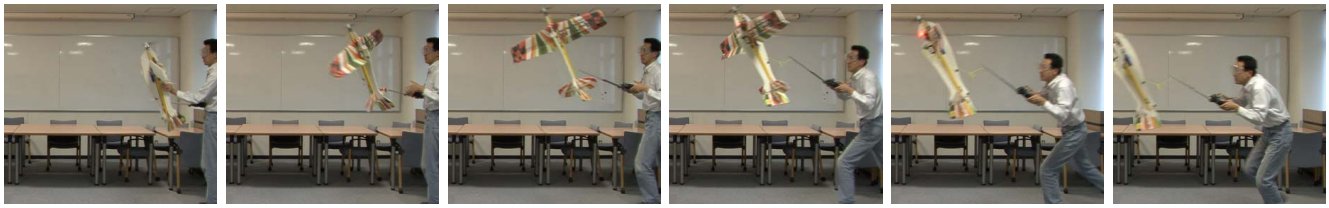

Fig. 10. Quaternion feedback control experiment. The UAV couldn't continue hovering.

Fig. 11. Resolved tilt-twist angle control experiment. Since large aileron angle caused drag force, the UAV lost altitude slightly. However, the UAV could continue hovering stably.

Fig. 14. Human inflicted rotational disturbance while hovering with resolved tilt-twist angle control, but the UAV continued hovering stably.

Fig. 15. Human inflicted translational disturbance while hovering with resolved tilt-twist angle control, but the UAV continued hovering stably.

VI. CONCLUSIONS

In this paper, we presented a novel hovering control strategy and applied it to PID controller to realize robust UAV hovering. The hovering control strategy is based on the analogy of an inverted pendulum model and composed of four steps. The two-dimensional UAV simulator was developed to evaluate the strategy. The resolved tilt-twist angle control achieves superior stability to quaternion feedback control when aircraft has large error angle around Z axis through simulation and experiment.

The application of the resolved tilt-twist angle feedback control for UAVs is not limited in hovering motion. It doesn't depend on any aircraft current and reference attitude. We believe it can be extended for many kind of aircraft maneuvers which dynamically shift attitude with stall condition, not just normal motion such as level flight.

VII. ACKNOWLEDGMENTS

This work was supported by Grant-in-Aid for Exploratory Research (No. 21656219), and Grant-in-Aid for JSPS Fellows (21-6015).

REFERENCES

[1] T. Cord, Air Force Research Laboratory, Wright-Patterson AFB: "SkyTote Advanced Cargo Delivery System," AIAA International Air and Space Symposium and Exposition: The Next 100 Years, AIAA-2003-2753, 2003.

[2] C. Schaefer, L. Baskett: "GOLDENEYE: The Clandestine UAV," 2nd AIAA Unmanned Unlimited Systems, Technologies, and Operations, AIAA-2003-6634, 2003.

[3] H. Stone and G. Clarke: "Optimization of Transition Maneuvers for a Tail-Sitter Unmanned Air Vehicle (UAV)," Australian International Aerospace Congress, pp. 105, 2001.

[4] H. Stone: "Control Architecture for a Tail-Sitter Unmanned Air Vehicle," Proceedings of the 5th Asian Control Conference, vol. 2, pp. 736-744, 2004.

[5] D. Kubo and S. Suzuki: "Tail-Sitter Vertical Takeoff and Landing Unmanned Aerial Vehicle: Transitional Flight Analysis," Journal of Aircraft, vol. 45, no. 1, pp. 292-297, 2008.

[6] W. E. Green and P. Y. Oh: "Autonomous Hovering of a Fixed-Wing Micro Air Vehicle," IEEE International Conference of Robotics and Automation, Orlando, FL, pp. 2164-2169, May 2006.

[7] W. E. Green and P. Y. Oh: "Optic-Flow-Based Collision Avoidance - Applications Using a Hybrid MAV," IEEE Robotics and Automation Magazine, vol. 15, no. 1, pp. 96-103, 2008.

[8] A. Frank, J. S. McGrewy, M. Valentiz, D. Levinex and J. P. How:"Hover, Transition, and Level Flight Control Design for a Single-Propeller Indoor Airplane," AIAA Guidance, Navigation and Control Conference and Exhibit, AIAA-2007-6318, 2007.

[9] N. B. Knoebel, S. R. Osborne, D. O. Snyder, T. W. McLain, R. W. Beard and A. M. Eldredge: "Preliminary Modeling, Control, and Trajectory Design for Miniature Autonomous Tailsitters," Proceedings of the AIAA Guidance, Navigation, and Control Conference and Exhibit, 2006.

[10] E. N. Johnson, M. A. Turbe, A. D. Wu, S. K. Kannan and J. C. Neidhoefer: "Flight Test Results of Autonomous Fixed-Wing UAV Transitions to and from Stationary Hover," Proceedings of the AIAA Guidance, Navigation, and Control Conference Exhibit, 2006.

[11] E. N. Johnson, A. Wu, J. C. Neidhoefer, S. K. Kannan and M. A. Turbe: "Flight-Test Results of Autonomous Airplane Transitions Between Steady-Level and Hovering Flight," Journal of Guidance, Control, and Dynamics, vol. 31, no. 2, pp. 358-370, 2008.

[12] K. Kita, A. Konno and M. Uchiyama:"Hovering Control of a Tail-Sitter VTOL Aerial Robot," Journal of Robotics and Mechatronics, Vol.21, No.2 pp. 277-283, 2009.

[13] B. Wie, H. Weiss and A. Arapostathis: "Quaternion Feedback Regulator for Spacecraft Eigenaxis Rotations," Journal of Guidance, Control and Dynamics, vol. 12, no. 3, pp. 375-380, 1989.